Characterization of EVA/Clay Nanocomposite Membranes and Its Pervaporation Performance

S. Anilkumar,*,† M. G. Kumaran,‡ and Sabu Thomas§

Department of Chemistry N. S. S. College, Ottapalam, Palakkad, Kerala, India, Rubber Research Institute of India Kottayam − 686009, Kerala, India, and School of Chemical Sciences, Mahatma Gandhi University, Priyadarshini Hills Po, Kottayam 686560 Kerala, India

Received: October 2, 2007; In Final Form: December 14, 2007

Pervaporation separation of chlorinated hydrocarbon/acetone mixtures has been investigated using nanoclay modified poly(ethylene-*co*-vinyl acetate) films. The results have been compared with the unfilled poly(ethylene-*co*-vinyl acetate) films. The nanoclay modified membranes were characterized by X-ray diffraction technique. The dispersion of layered silicates in the polymer matrix was analyzed using transmission electron microscopy. The nanoclay showed excellent dispersion in the polymer matrix. The effect of free volume on the pervaporation performance was investigated by positron annihilation lifetime spectroscopy. Poly(ethylene-*co*-vinyl acetate) nanocomposite membrane showed high selectivity because of the plateletlike morphology and high aspect ratio of layered silicates. The nano clay content and the swelling effects on pervaporation performance of nano composite membranes have been investigated in detail.

1. Introduction

Pervaporation (PV) is an efficient membrane based process which has gained acceptance by chemical industries over the years because of its favorable economics, easy maintenance, and simplicity of the process.[1−5] The pervaporation process can be defined as a selective evaporation of a liquid mixture through a dense polymeric membrane.[6] It can play an important role in the separation of volatile liquid mixtures when a very low concentration of one component or the presence of azeotropic composition hinders a complete separation through distillation. The main applications include the dehydration of organic solvents,[7] the removal of trace volatile organic compounds from aqueous solution,[8] and the separation of organic−organic mixtures.[9] High permeability, good selectivity, and stability are the important factors in choosing suitable pervaporation membranes.

Polymer−clay nanocomposites are hybrid composite materials consisting of a polymer matrix with dispersed clay nanoparticles. Nanoclays have been widely used as an inorganic reinforcement for polymer matrixes with nanoscale dispersion of the inorganic phase within the polymer matrix.[10−14] Addition of nanoclay to polymer can lead to higher moduli,[15−17] increased strength and heat resistance,[15−17] and decreased gas permeability[18] and flammability.[19] The enhanced properties are presumably due to the nanoscale structure effects and the interaction between inorganic and organic materials. The permeability performance of nanocomposite normally depends on the clay content, aspect ratio, and degree of dispersion of silicate layers.[20] The permeability reduction was attributed to extremely high aspect ratio of clay platelets, which increased the tortuosity of the path of gas or solvent molecules as molecules diffused into the nanocomposite. Okada et al.[21] reported the decrease in moisture permeability for nanoclay polyamide composites. The gas permeability of rubber clay hybrid was reduced by 30% with 4 volume % of exfoliated clay.[22] Guo et al.[23] prepared novel poly vinyl alcohol (PVA)/silica nanocomposite membranes for the pervaporation of ethylene glycol aqueous solution and found that when 50 wt % of the silica was added to poly(vinyl alcohol) the nanocomposite membranes possessed optimum pervaporation performance. Naidu et al.[24] reported the pervaporation separation of water−isopropanol mixtures through nanocomposite poly(vinyl alcohol) membranes. It was found that addition of a small amount of nanoparticles to PVA membrane will increase the selectivity to infinity values. Polyamide/nanoclay composite membranes were prepared and used for the separation of water−ethanol mixture by Wang et al.[25]

In this study, poly(ethylene-*co*-vinyl acetate) (EVA) nanoclay composite films were prepared. The pervaporation characteristics of these films using chloroform−acetone mixtures were analyzed and compared with unfilled EVA membranes. Nanostructure morphology was studied using X-ray diffraction and transmission electron microscopy. The influence of the weight percentage of filler on pervaporation was also investigated. In our former paper, we reported that cross-linked EVA membranes can be effectively used for the separation of chlorinated hydrocarbon/acetone mixtures.[26] The effect of free volume on the pervaporation performance was investigated by positron annihilation lifetime spectroscopy.

2. Experimental Section

2.1. Materials. Poly(ethylene-*co*-vinyl acetate), EVA (Pilene 1802), was obtained from Polyolefin Industries Limited, Chennai, India. The cross-linking agent used was dicumyl peroxide (DCP). The nanoclay, cloisite Na^+, was obtained from Southern Clay Products, United States. The cation exchange capacity of the clay is 92.6 meq/100 g, and its specific gravity is 2.86 g/cm^3. It contains no organic modifier. The solvents, chloroform, and acetone used in this study were obtained from E-Merck (India) Ltd, Mumbai, India, and were of reagent grade.

* To whom correspondence should be addressed. Tel.: 09446045664. Fax: 91 481 561 190/800. E-mail: anugraha_anil@yahoo.co.in.
† Department of Chemistry N. S. S. College.
‡ Rubber Research Institute of India Kottayam.
§ Mahatma Gandhi University.

10.1021/jp7096444 CCC: $40.75
Published on Web 03/12/2008

2.2. Membrane Fabrication. Unfilled and nanoclay modified EVA membranes were prepared. Dicumyl peroxide (DCP) was used as the curing agent. The amount of DCP used was 1 gm. The mixing was done in a two-roll mixing mill at a nip gap of 1.3 mm and at a friction ratio of 1:1.4. The nip gap, mill speed ratio, time of mixing, and temperature of the rolls were kept constant for all mixes. The vulcanization behavior of the samples was studied by using a Monsanto Rheometer. The sheeted out stock was compression molded in a hydraulic press at 160 °C under a load of 24.5×10^4 N. The samples are designated as F_0, F_3, F_5, and F_7, where the subscript numbers represent the number of grams of nanoclay used per 100 grams of the polymer.

2.3. Membrane Characterization. *2.3.1. X-ray Diffraction Analysis.* X-ray diffraction patterns were taken by using Ni-filtered Cu K∞ radiation ($\lambda = 0.154$ nm) by X'pert diffractometer, Philips at 40 kev and 30 mA. The samples were scanned in step mode by 1.5°/min scan rate. Throughout the investigation, the operating voltage and the current of the tube were maintained constant.

2.3.2. Transmission Electron Microscopic Analysis. Transmission electron microscopy (TEM) is the most important method for the analysis of dispersion of layered silicates in polymer nanocomposites. The dispersion of layered silicates in EVA matrix has been investigated by TEM. Transmission electron micrographs of the nanocomposites were taken in a Leo 912 Omega transmission electromicroscope with an acceleration voltage of 120 kev. The specimens were prepared using an ultracut E cryomicrotone. Thin sections of about 100 nm were cut with a diamond knife at −120 °C.

2.3.3. Positron Annihilation Lifetime Spectroscopic Analysis. Positron annihilation lifetime spectra (PALS) is used to examine the free volume present in unfilled and nanofilled EVA samples. The positron lifetime spectrometer consists of a fast−fast coincidence system with BaF_2 scintillators coupled to photomultiplier tubes type XP2020/Q with quartz window as detectors. The detectors were shaped to conical to achieve better time resolution. A 17 m Ci ^{22}Na positron source, deposited on a pure Kapton foil of 0.0127 mm thickness, was placed between two identical pieces of sample under investigation. This sample−source sandwich was positioned between the two detectors of PALS to acquire lifetime spectrum. The spectrometer measures 180 ps as the resolution function with ^{60}Co source.

However, for better count rate, the spectrometer was operated at 220 ps time resolution.[27] All lifetime measurements were performed at room temperature and two to three positron lifetime spectra with more than a million counts under each spectrum were recorded. In PALS analysis, only two parameters were measured, namely, o-Ps lifetime (τ_3) and o-Ps intensity I_3. The o-Ps lifetime τ_3 measures the size of the free-volume holes (V_f), and I_3 is a relative measure of the number of free-volume sites in the polymer matrix.

The free-volume cavity radius (R) is related to the o-Ps pick-off lifetime (τ_3) by a simple relation. The underlying assumption in the formulation of this relation is that o-Ps atom in a free-volume cell can be approximated to a particle in a potential well of radius R_0. The potential is infinite if $r > R_0$ and is constant for $r \leq R_0$. Further, it is assumed that there is an electron layer in the region $R < r < R_0$ with $R_0 = R + \delta R$ where δR represents the thickness of the electron layer or the probability of the overlap of P_s wave function and electron wave function. The expression relating the free-volume radius R (in nm) and the o-P_s pick-off lifetime τ_3 (in ns) according to Nakanishi et al.[28] is

$$\left(\frac{1}{\tau_3}\right) = 2\left[1 - \left(\frac{R}{R_0}\right) + \left(\frac{1}{2\pi}\right)\sin\left(\frac{2\pi R}{R_0}\right)\right] \quad (1)$$

Here, the value of $\delta R = 0.1656$ nm was determined by fitting experimental τ_3 values to data from molecular materials with well-known hole size like zeolites.[29] Using this value of R, the free-volume size (V_f) is calculated as $V_f = (4/3)R^3$. Then, the relative fractional free volume is evaluated as the product of free volume (V_f) and o-P_s intensity, I_3 (%).

2.3.4. Swelling Experiments. Samples of dry membranes of known weight were immersed in pure solvent and were allowed to equilibrate for 72 h. The swollen membrane was taken out and was wiped with tissue paper to remove adherent solvent and then was weighed. The swelling ratio was calculated using the equation[26]

$$S = \frac{W_s - W_d}{W_d} \quad (2)$$

where W_d denotes the weight of the dry membrane and W_s denotes the weight of solvent swollen membrane.

2.3.5. Pervaporation. The schematic representation of the pervaporation apparatus has been described in the previous paper.[26] The permeation cell is assembled from two half cells of column couplers made of glass and fastened with bolted clamps. The capacity of each cell was about 100 mL and the effective area of the membrane was 19.4 cm^2. The membrane was supported on a finely porous stainless steel plate with holes drilled in it. Vacuum at the downstream side was measured with a vacuum gauge. The membrane was kept in the pervaporation cell for about 2 h in each run to reach equilibrium conditions before collecting the permeate. The permeated vapors were completely condensed in a trap placed in a Dewar Flask cooled to −77 °C using dry ice−acetone mixture. The permeate and feed composition were analyzed by gas liquid chromatography. Pervaporation experiments were carried out in triplicate at 30 °C using freshly prepared feed solution each time to check the reproducibility of measurements.

Performance of a membrane in pervaporation is characterized by permeation rate or flux (J) and selectivity. The flux can be calculated from the weight of the permeate collected after pervaporation run from the following equation:[30]

$$J = \frac{Q}{At} \quad (3)$$

where Q is the quantity in kilograms of permeate collected after a time (t) and A is the effective area of the membrane.

The selectivity (α_{perv}) is defined as[31]

$$\alpha_{perv} = \frac{(Y_i/Y_j)}{(X_i/X_j)} \quad (4)$$

where Y_i and Y_j represent the weight fraction of chlorinated hydrocarbon and acetone in the permeate, and X_i and X_j represent those of chlorinated hydrocarbon and acetone in the feed, respectively.

The overall selectivity is a combination of the effects of the membrane (sorption−diffusion selectivity) and the volatility or evaporative selectivity. If the downstream pressure is negligible, the apparent separation factor or selectivity is given by[32]

$$\alpha_{perv} = \alpha_{mem} \cdot \alpha_{evap} \quad (5)$$

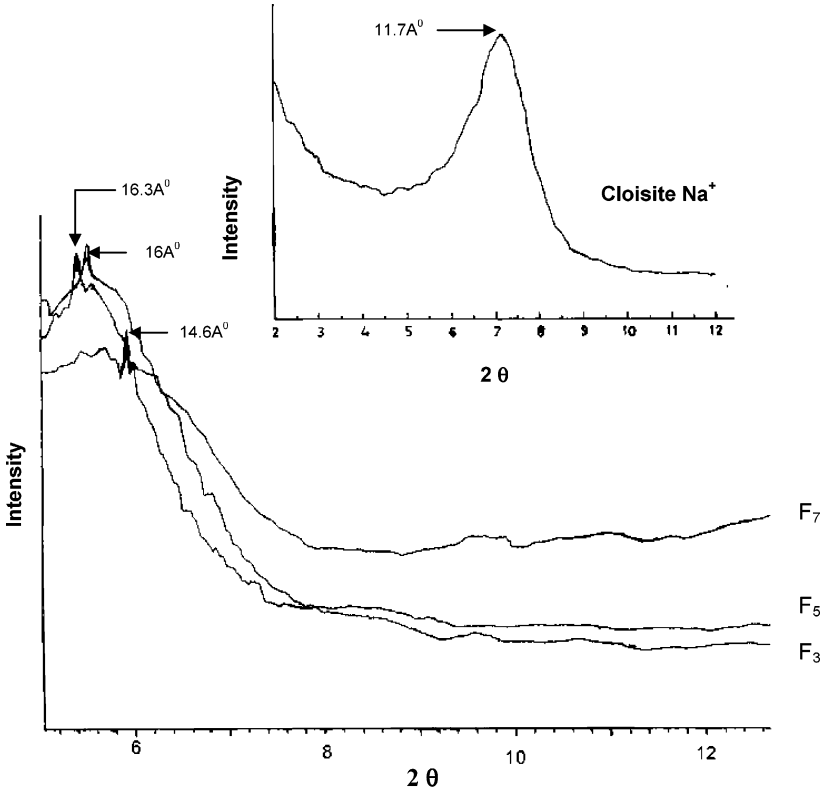

Figure 1. X-ray diffraction patterns of nanoclay and EVA clay nanocomposites.

The membrane selectivity (α_{mem}) and the evaporative selectivity (α_{evap}) is given by the equations.[31]

$$\alpha_{mem} = \frac{(P_i)}{(P_j)} \tag{6}$$

$$\alpha_{evap} = \frac{p_i\gamma_i}{p_j\gamma_j} \tag{7}$$

where P refers to the permeability and p, γ refers to vapor pressure and activity coefficient of the components i and j. The membrane selectivity (α_{mem}) can be calculated using eq 5.

3. Results and Discussion

3.1. X-ray Diffraction Analysis (XRD). The X-ray diffraction patterns of the nanoclay and polymer nanocomposites are shown in Figure 1. Cloisite Na^+ clay exhibits a single peak at an angle 2θ of 7° corresponding to a d-spacing of 11.7 A°. For EVA/clay nanocomposites, the characteristic diffraction peak moves to a lower angle with respect to that of nanoclay. For the composite samples containing 3 (F_3), 5 (F_5), and 7 (F_7) wt % of clay, the d-spacings were 16.3, 16, and 14.6 A° corresponding to 2θ 5.4, 5.5, and 6.04°, respectively. This shows that EVA chains have intercalated into the interlayers of cloisite Na^+. It is found that in all systems the interlayer spacing increases because of the intercalation of polymer into the layers of nanoclay. Enhanced interlayer distance indicates that the layered structure is retained. With the increase of clay content, the left shift magnitude of diffraction peak decreases, that is, the enlargement extent of the interlayer distance of the clay decreases. This indicates that the lower the loading of nanoclay the more favorable is the intercalation of EVA chains into the silicate layers.

3.2. Transmission Electron Microscopic Analysis (TEM). The transmission electron micrographs of various EVA−clay nanocomposites are presented in Figure 2. The dark lines in the transmission electron micrographs show the dispersion of silicates in the polymer matrix. It can be seen that in the F_3 sample, the clay is well dispersed in the matrix and has a more ordered exfoliated structure. When the percentage of clay increases, dispersion decreases and clay exists as large aggregates and is unable to undergo exfoliation. The above observation is consistent with the data observed from the XRD patterns given in Figure 1.

3.3. Positron Annihilation Lifetime Spectroscopic Analysis (PALS). Free volume present in nanocomposite systems plays a major role in determining the overall performance of the membranes. PALS is an efficient technique used for the analysis of free volume. The diffusion of permeant through polymeric membranes can be described by two theories, namely, molecular and free-volume theories. According to the free-volume theory, the diffusion is not a thermally activated process as in the molecular model, but it is assumed to be the result of random redistributions of free-volume voids within a polymer matrix. Cohen and Turnbull[33] developed the free-volume models that describe the diffusion process when a molecule moves into a void larger than a critical size, V_c. Voids are formed during the statistical redistribution of free volume within the polymer. The effect of layered silicates on o-Ps lifetime (τ_3), o-Ps intensity (I_3%), and relative fractional free volume percentage is presented in Table 1. It can be seen from the table that the relative fractional free volume percentage is lowest for F_3 system. It is found that the relative fractional free volume of unfilled polymer decreases on the addition of layered silicates. The decrease is attributed to the interaction between layered silicate and polymer because of the platelet structure and high aspect ratio of layered silicates. The decrease is explained to the restricted mobility of the chain segments in the presence of layered silicates. This results in reduced free-volume concentration or relative fractional free volume. The contact surface area between the filler

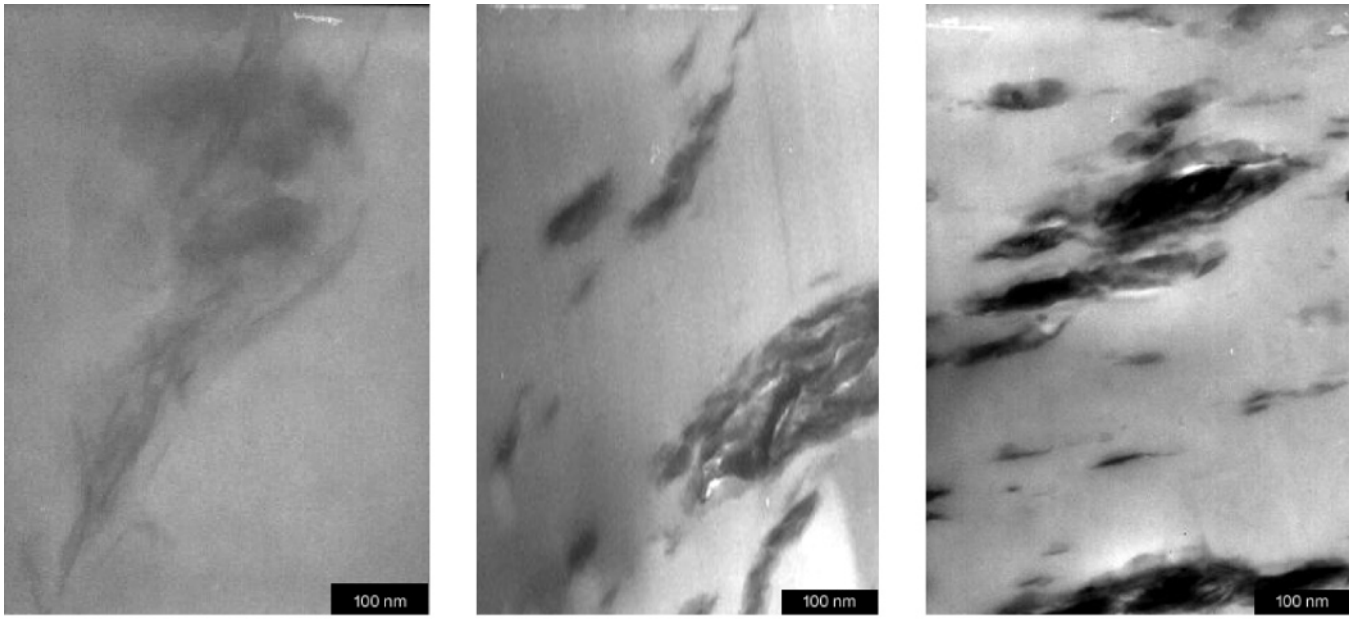

Figure 2. TEM images of nanocomposites (a) F_3, (b) F_5, and (c) F_7.

TABLE 1: PALS Measurement Data of Nanocomposites

sample	*o*-P_s lifetime ($\tau_3 \pm 0.01$ ns)	*o*-P_s intensity ($I_3 \pm 0.1\%$)	relative fractional free volume %
F_0	2.33	20.48	4.78
F_3	2.38	7.29	1.77
F_5	2.35	14.61	3.46
F_7	2.32	17.85	4.13

and the matrix is higher in nanocomposites owing to its high aspect ratio, which in turn reduces the free-volume concentration. It is also found that the relative fractional free volume percentage increases with clay loading. The increase in the values of fractional free volume can be attributed to the aggregation of fillers and the consequent additional void formation. The impact of nanoparticles on the free volume and the barrier properties has been studied by Wang et al.[12] and Stephen et al.[11] They have concluded that the permeability of nanocomposite is mainly influenced by fractional free volume effects.

3.4. Swelling Ratio. The swelling ratio values of unfilled and nanoclay modified EVA films are presented in Figure 3. The unfilled membrane (F_0) showed maximum swelling ratio value for all feed concentrations. Modified EVA films with 3 wt % of nanoclay (F_3) showed the minimum, and the value increases with increase in weight percentage of the filler.

The two main factors that influence the swelling of the films are the availability of free volume in the polymer and the chemical compatibility between the polymer chain and the solvent mixture. A higher material volume accessible for the liquid sorption and a higher flexibility of the network allow an increased solvent uptake for the unfilled sample.

The decreased swelling ratio values of modified EVA films (F_3) is explained as follows. The impermeable clay layers dictate a tortuous pathway for the permeate to pass through the nanocomposite. The reduced swelling of nanocomposites is influenced by two factors, namely, geometry of the filler and the molecular level interaction of the matrix and filler. Because of the plateletlike morphology of silicates, the nanofilled matrix exhibits reduced permeability owing to increase in the tortuosity

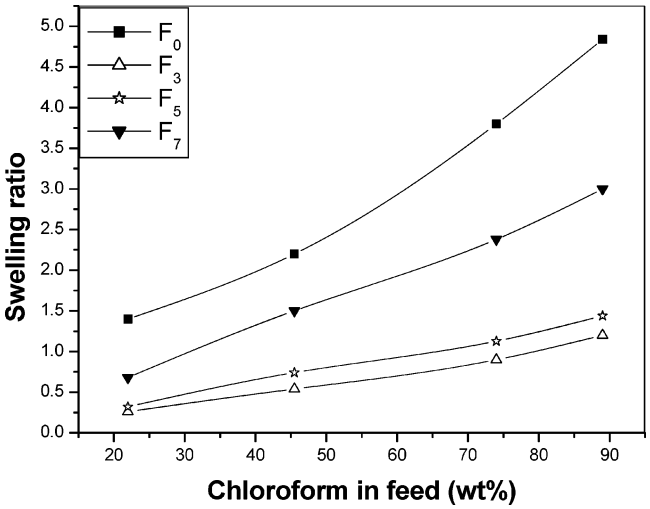

Figure 3. Swelling ratio of unfilled and EVA nanocomposite films.

of the path. Because of the high aspect ratio, the nanofillers exhibit more exfoliated structure. Therefore, F_3 system exhibited reduced swelling because of high polymer/filler interaction resulting in reduced free volume. The swelling ratio of composites increases as a function of filler loading. This can be explained in terms of aggregation of fillers with increase in the concentration of filler. This resulted in the weakening of the polymer chains. The diffusion path is schematically represented in Figure 4.

From Figure 4a, it is clear that, as in the case of the microcomposite, the penetrant molecules can easily pass through the interphase between the filler and the matrix. However, in the case of clay-filled nanocomposite (Figure 4b), the penetrant molecule experiences a difficult pathway because of molecular level dispersion of clay in the matrix.

3.5. Pervaporation of Chloroform−Acetone Mixtures. The pervaporation performance of unfilled and nanocomposite membranes were analyzed using chloroform−acetone mixtures. Both unfilled and nanoclay modified membranes showed chloroform selectivity from chloroform−acetone mixtures. The

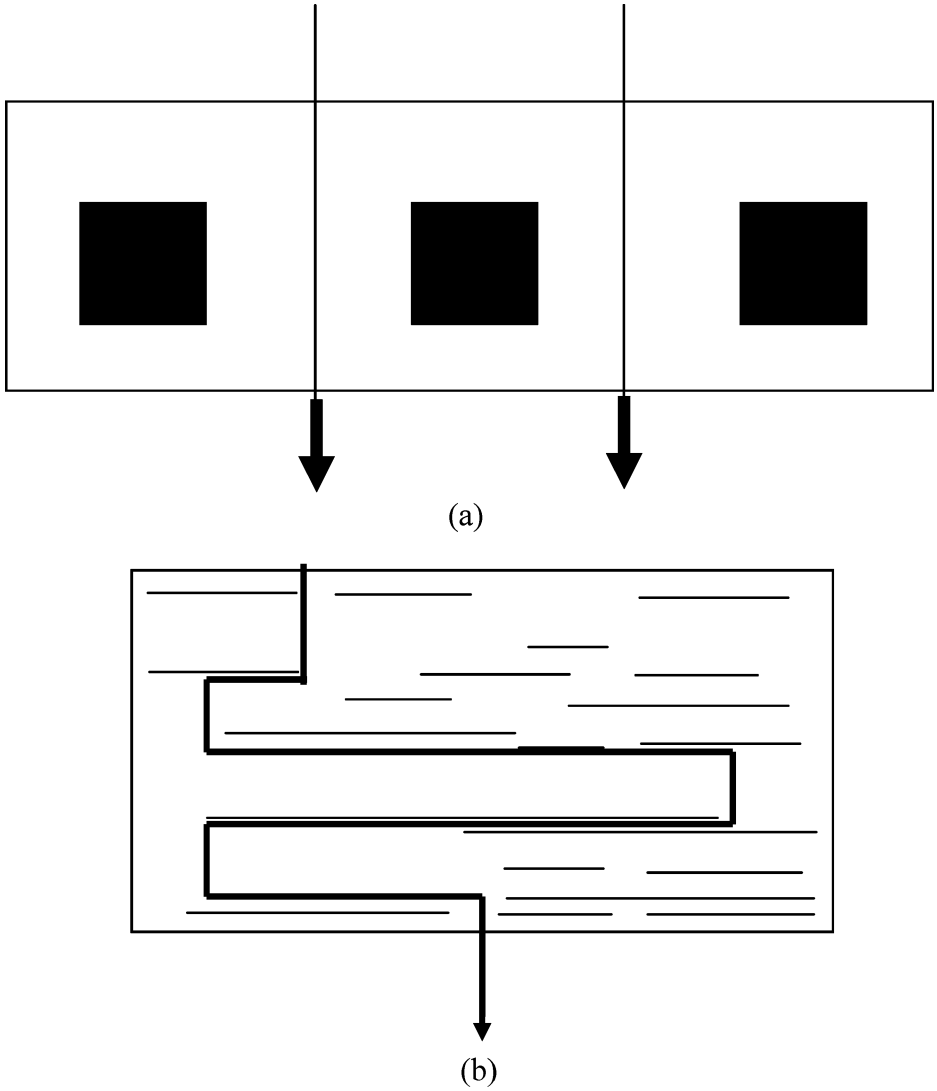

Figure 4. Schematic representation of diffusion through (a) composite with conventional filler and (b) nanocomposites.

TABLE 2: Pervaporation Characteristics of EVA Films (22 wt % of Chloroform−Acetone Mixture)

system	permeation composition (wt %)	selectivity α_{ij}	flux (kg/m^2 h)
F_0	52	3.8	0.27
F_3	91	36	0.12

affinity of EVA membranes toward chloroform is higher than acetone, and this creates a remarkable difference in the separation of chloroform from chloroform−acetone mixtures.[26]

Table 2 shows the permeation rate and the selectivity of unfilled (F_0) and modified films with 3 wt % of filler (F_3). EVA/clay nanocomposite membrane showed a higher selectivity but a lower permeation rate than the unfilled ones. Composites containing 3 wt % of filler showed maximum solvent selectivity which is almost 10 times higher than that of unfilled ones. The increased selectivity is due to the exfoliation of silicates in the polymer matrix leading to the nanometric level dispersion of the organic and inorganic phases. The molecular level of polymer/filler interaction results in a reduced availability of free volume, and as a result, the permeation rate decreases and the separation factor increases. The enhanced selectivity of nano-filled membranes is because of their plateletlike morphology and high aspect ratio of the fillers. Because of the high aspect ratio of layered silicates, the contact area between the filler and the matrix increases. Hence, there will be more resistance toward molecular diffusion resulting in a reduced permeation rate. The above results have been complemented by PALS analysis.

3.6. Influence of Nanoclay Loading. The influence of the weight percentage of nanoclay on pervaporation performance is given in Figure 5. A composition of 45.5% chloroform−acetone mixture is used. It is found that selectivity increases, reaches a maximum, and then decreases with clay loading. It is also found that all nanocomposite membranes showed a higher selectivity than the unfilled one. However, the selectivity factor decreases sharply when the clay content becomes higher than 3 wt %. This can be explained in terms of aggregation of clay particles at higher clay loading. When the clay composition is greater than 3 wt %, the compatibility of the filler and the matrix decreases, resulting in microphase separation. PALS analysis also showed that the fractional free volume percentage decreases at higher clay loading. Hence, a drop in selectivity and an increase in permeation rate was observed. Wang et al.[25] investigated the effect of clay content on the pervaporation performance of 90 wt % aqueous ethanol solution through the polyamide/clay nanocomposite membrane. They found that selectivity decreases sharply when the clay content becomes higher than 2 wt %.

3.7. Calculation of Membrane Selectivity (α_{mem}). The membrane selectivity, α_{mem}, is calculated for unfilled (F_0) and nanocomposite membrane (F_3) using eq 5. The values of

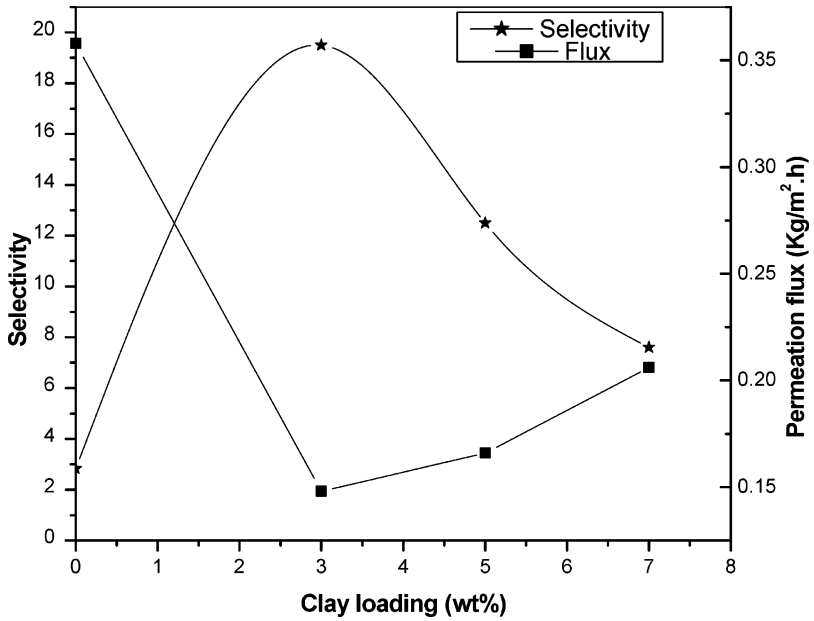

Figure 5. Influence of filler loading on pervaporation.

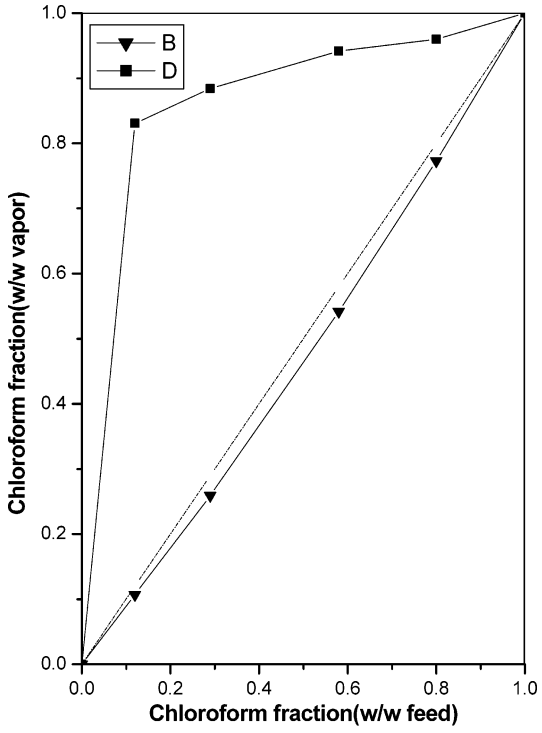

Figure 6. Comparison of vapor−liquid equilibrium curve with pervaporation data for nanocomposite films. B, vapor composition of the permeate; D, liquid−vapor equilibrium curve.

TABLE 3: Membrane Performance (22 wt % of Chloroform Mixture)

sample	α_{mem}	α_{ev}
F_3	72.5	0.49
F_0	6.6	0.49

membrane selectivity will provide an interesting study of how a mass-separating agent can overcome the intrinsic volatility differences and can enable to permeate the less volatile component in a mixture. Table 3 gives the membrane selectivity for unfilled and nanocomposite membrane. It can be seen from the table that the evaporative selectivity is being overcome by the membrane selectivity. The membrane selectivity is much higher for nanoclay modified EVA membranes.

3.8. Comparison of Pervaporation Results with Vapor−Liquid Equilibrium (VLE) Data. Chloroform and acetone form an azeotrope at 80 wt % of chloroform. Separation of azeotropes by simple distillation is possible only by adding a third component, that is, an entrainer such as benzene, which is known as a deadly carcinogen. In the membrane based pervaporation separation, the membrane acts as a third phase to break the azeotrope. Thus, pervaporation is more effective in separating azeotropes than conventional distillation is. Figure 6 shows that the pervaporation curve is higher than that of the vapor−liquid equilibrium (VLE) curve throughout the composition range of the feed mixture.

4. Conclusions

Poly(ethylene-*co*-vinyl acetate)−clay nanocomposites containing different filler loadings have been prepared, and the pervaporation features of the membranes were investigated. Morphology of the composite membranes were analyzed by X-ray diffraction and transmission electron microscopy. It has been found that the diffraction peaks were shifted to lower angles with an increase in *d*-spacing. Samples with 3 wt % of filler showed maximum increase in *d*-spacing. Transmission electron microscopic images showed that sample with 3 wt % of clay showed excellent dispersion of clay particles resulting in an exfoliated structure. The dispersion of nanoparticles decreases with an increase in clay loading. The fractional free volume percentage was determined using positron annihilation lifetime spectroscopic analysis. Sample with 3 wt % clay showed the least free volume. Pervaporation studies showed a far superior performance in solvent selectivity in the case of the filled system compared to the unfilled one. Composites containing 3 wt % filler showed maximum solvent selectivity which is almost 10 times higher than that of unfilled ones. However, an increase in flux and a decrease in selectivity were observed when the clay content became higher than 3 wt %. The developed membranes could break the azeotrope containing 80% chloroform.

Acknowledgment. The authors are thankful to DST, New Delhi for the financial support of the project.

References and Notes

(1) Fleming, H. L. *Chem. Eng. Prog*. **1992**, *7*, 46.
(2) Huang, Z.; Shi, Y.; Wen, R.; Guo, Y. H.; Fengsu, J.; Matsura, T. *Sep. Purif. Technol.* **2006**, 51, 126.
(3) Chapman, P. D.; Tan, X.; Andrew, K. G.; Livingston; Oliveira, T. *J. Membr. Sci.* **2006**, *268*, 13.
(4) Katarzynski, D.; Staudt, C. *Desalination* **2006**, *200*, 23.
(5) Bengston, G.; Oeuring, M.; Fritsch, D. *Chem. Eng. Process.* **2004**, *43*, 1159.
(6) Gozzelino, G.; Malucelli, G. *Colloids Surf., A: Physiochem. Eng. Aspects* **2004**, *235*, 35−44.
(7) Brookes, P. R.; Livingston, A. G. *J. Membr. Sci.* **1995**, *104*, 119.
(8) Yeon, C.; Lee, K. H. *J. Membr. Sci.* **1996**, *109*, 251.
(9) Hao, J.; Tanaka, K.; Kita, H.; Okamoto, K. *J. Membr. Sci.* **1997**, *132*, 97.
(10) Takahashi, S.; Paul, D. R. *Polymer* **2006**, *47*, 7535.
(11) Stephen, R.; Ranganathaiah, C.; Varghese, S.; Joseph, K.; Thomas, S. *Polymer* **2006**, *47*, 858−870.
(12) Wang, Z. F.; Wang, B.; Qi, N.; Zhang, H. F.; Zhung, L. Q. *Polymer* **2005**, *46*, 719.
(13) Hedenqvist, M. S.; Backman, A.; Gallstedt, M.; Boyd, R. H.; Gedde, U. W. *Compos. Sci. Technol.* **2006**, *241*, 156−166.
(14) Heinz, H.; Vaia, R. A.; Krishnamoorti, R.; Farmer, B. L. *Chem. Mater.* **2007**, *19*, 59−68.
(15) Vaia, R. A.; Teukolsky, R. K.; Giannelis, E. P. *Chem. Mater*. **1994**, *6*, 1017−1022.
(16) Vaia, R, A.; Giannelis, E. P. *Macromolecules* **1997**, *30*, 7990−7999.
(17) Vaia, R. A.; Giannelis, E. P. *Macromolecules* **1997**, *30*, 8000−8009.
(18) Osman, M. A.; Rupp, J. E. P.; Suter, U. W. *J. Mater. Chem*. **2005**, *15*, 1298−1304.
(19) Manias, E.; Touny, A.; Wu, L.; Strawchecker, K.; Lu, B.; Chung, T. C. *Chem. Mater.* **2001**, *13*, 3516−3523.
(20) Kim, J. K.; Hu, C.; Woo, R. S. C.; Sham, M. L. *Compos. Sci. Technol.* **2005**, *65*, 805−813.
(21) Okada. A.; Kawasumi. M.; Usnki. A.; Kojmova. Y.; Kuraucha. P.; Kamigityo. O. *Mater. Res. Soc. Proc.* **1990,** *171*, 45 − 50.
(22) Lan, T.; Pinnavaia, T. J. *Chem. Mater*. **1994,** *6*, 2216−2224.
(23) Guo, R.; Ma, X.; Hu, C.; Jiang, Z. *Polymer* **2007**, *48*, 2939.
(24) Naidu, B. V.; Sairam, M.; Raju, K. V. S. N.; Aminabhavi, T. M. *J. Membr. Sci.* **2005**, *260*, 142.
(25) Wang, Y. C.; Fan, S. C.; Lee, K. R.; Li, C. L.; Huang, S. H.; Tsai, H. A.; Lai, J. Y. *J. Membr. Sci.* **2004**, *239*, 219−226.
(26) Anilkumar, S.; Gedam, P. H.; Kishan Prasad, V. S.; Kumaran, M. G.; Thomas, S. *J. Appl. Polym. Sci.* **1996**, *60*, 735−741.
(27) Ravikumar, H. B.; Ranganathaiah, C.; Kumaraswamy, G. N.; Thomas, S. *Polymer* **2005**, *46*, 2372.
(28) *Positron and Positronium Chemistry;* Nakanishi, H., Jean, Y. C., Schrader, D. M., Jean, Y. C., Eds.; Elsevier: Amsterdam, 1988; p 159.
(29) Jean, Y. C. *J. Microchem.* **1990**, *42*, 72.
(30) Das, S.; Banithia, A. K.; Adhikari, B. *J. Membr. Sci.* **2006**, *280*, 675 − 684.
(31) Xu, W.; Paul, D. R.; Kores, W. J. *J. Membr. Sci.* **2003**, *219*, 89−102.
(32) Wijmans, J. G.; Baker, R. W. *J. Membr. Sci.* **1993**, *79*, 101−113.
(33) Turnbull, D.; Cohen, M. H. *J. Chem. Phys.* **1961**, *34*, 120.